Korean J. Chem. Eng., 32(5), 867-873 (2015)
DOI: 10.1007/s11814-014-0278-x

pISSN: 0256-1115
eISSN: 1975-7220

Carbide-derived carbon/sulfur composite cathode for multi-layer separator assembled Li-S battery

Sun-Hwa Yeon*,†, Wook Ahn*,, Kyoung-Hee Shin*, Chang-Soo Jin*, Kyu-Nam Jung*, Jae-Deok Jeon*, Sungnam Lim***, and Youngchul Kim****

*Korea Institute of Energy Research, 102, Gajeong-ro, Yuseong-gu, Daejeon 305-343, Korea
**Department of Materials Science & Engineering, Yonsei University, 50, Yonsei-ro, Seodaemun-gu, Seoul 120-749, Korea
***Department of Chemical and Biomolecular Engineering, KAIST, 373-1, Guseong-dong, Yuseong-gu, Daejeon 305-701, Korea
****Agency for Defense Development, Yuseong-gu, P. O. Box 35-4, Daejeon 305-600, Korea
(*Received 26 March 2014 • accepted 21 September 2014*)

Abstract−To improve the electrochemical performance of Li-S rechargeable batteries, tunable porous carbon materials, which are known as carbide-derived carbons (CDCs), are employed as adsorbents and conductive matrices for the cathodic sulfur materials. A new assembly for Li-S cells was developed by introducing multi-layer membranes as separators. The use of the multi-layer membranes enables the minimization of the shuttle effect by expanding the distance between the separators and blocking the penetration of the polysulfide. The best discharge capacity and cycle life were obtained with ten layers of PP membrane in a sulfur-CDC@1200 composite cathode, resulting in a discharge capacity of 670 mA h g^{-1} and a minimal gap in the charge-discharge capacity during cell cycling.

Keywords: Li-S Battery, Carbide-derived Carbon, Multi-layer Membrane

INTRODUCTION

Sulfur (S) has many valuable characteristics, such as a low equivalent weight, extremely low cost, and nontoxicity. In a Li-S cell, the potential corresponds to 1/2-2/3 of the potential exhibited by a typical positive electrode for a Li-ion cell (3.2 V-4.2 V). However, this low potential is outweighed by the 1,672 mA h g^{-1} theoretical specific capacity, which is the highest of all known solid cathode materials [1].

Porous carbon possesses a high adsorption capacity when used as a storage medium and is the best active sorbent material for the cathodes in Li-S batteries. Recently developed carbon-sulfur cathodes in Li-S batteries have achieved enhanced stability by incorporating carbon nanotubes/nanofibers, graphene, mesoporous carbon, microporous carbon, and hierarchical porous carbon [2-7]. Particularly, microporous carbon has been highlighted as the most promising material for the sulfur cathode because it allows the creation of a homogeneous-amorphous composite via the doping of sulfur on microporous carbon. This material displays excellent cyclability because it maintains high porosity, even after the formation of the composite state [8]. However, while microporous carbon has an advantageous high specific surface area (SSA), its numerous pores cause low electrical conductivity. Therefore, control of the structure and porosity are required to develop good electrical conductivity within Li-S batteries. Previous studies revealed a high electrochemical capacity (680 mAh g^{-1}) was enabled with low sulfur loaded-porous MSP carbon (~25 wt% S) as the Li-S cathode [9]. Unlike commercial microporous carbon (MSP-20), carbide-derived carbons (CDCs) are a type of carbon with easily tuned proper structures, as well as intrinsic carbon structures that can be controlled via selective etching of crystalline metal carbides and temperature control during synthesis [10]. CDCs are possible candidates for use in Li-S batteries because their pore structures and highly ordered crystalline phases can simultaneously be controlled by modulating the conditions during synthesis.

In Li-S batteries, the dissolution of polysulfides in the electrolyte during the discharge-charge process causes redox shuttling between the anode and cathode, triggering severe loss of usable active material [11,12]. Once the Li anode is fully coated, S_n^{2-} reacts with these reduced sulfides to form lower order polysulfides (S_{n-x}^{2-}), which become concentrated on the anode side. Additionally, after charging, the soluble polysulfide irreversibly deposits as lithium sulfide on the cathode surface to hinder lithium ion migration, deteriorate the electrode through sulfur poisoning, and reduce the electrode's conductivity. These severe issues degrade the capacity when the system is subjected to a large current and lead to poor cycling stability. To solve these problems, the formation of a sulfur composite framework and physical cell assembly has been attempted in the cathode, electrolyte, and anodes. A non-carbonate-containing solvent-based electrolyte [13] with an additive $LiNO_3$ salt form the best electrolyte because the additive salt can prevent the polysulfide shuttling or reduce the solubility of the polysulfide. The addition of $LiNO_3$ improves the cyclic performance of Li-S cells to some extent [14]. However, in spite of the improvements caused by the additive, the large gap between the discharge and charge capacities during cycling remains an unsolved problem for diverse sulfur composites at high sulfur loading.

In this study, we reveal porous S-CDC composite cathodes that

†To whom correspondence should be addressed.
E-mail: ys93@kier.re.kr

can improve the cyclability of Li/S batteries at high sulfur loading. Additionally, a new Li-S cell assembly is proposed to minimize the polysulfide crossover during the discharge-charge. The multi-layered separators enable the attenuation of the shuttling effect, preventing the penetration of the polysulfide during operation. Therefore, the new Li-S cell delivers improved charge-discharge cyclability by inhibiting the precipitation of solid Li_2S_2 and Li_2S.

EXPERIMENTAL

1. Preparation of Cathode

CDC powders were produced by chlorinating TiC powder (particle size 1-4 μm). This precursor was placed in a horizontal tube furnace, purged in argon flow, and heated to 1,200 °C under flowing chlorine (10-15 cm^3 min^{-1}) for 3 h. CDC powders were then annealed at 600 °C for 2 h under flowing hydrogen to remove residual chlorine and chloride trapped in pores. Previous studies showed that this procedure was not necessary at higher hydrogenation temperatures [10]. We denoted the prepared CDCs as CDC@1200, according to chlorination temperature, for example 1,200 °C. The elemental S powder was purchased from Sigma Aldrich (100 mesh particle size, reagent grade). The S loading procedures are as follows. **S-impregnation (IS) method**: S powder was dissolved in a CS_2 solution to form a 10 wt% S solution. The 10 wt% S solution was added dropwise to a CDC matrix with the same pore volume as the volume of solution with vigorous mixing. After the addition was complete, the matrix was slightly wet. Immediately afterwards, the resulting precursor was dried for 16 h at 60-70 °C. We denoted the S-carbon composites prepared by the IS process as S-CDC@1200 composites, in which the S loadings were 25 wt%-50 wt%.

2. Characterization

Gas adsorption analysis was performed using BELSORP-Max MP (BEL Japan Inc.) with N_2 adsorbate at −196 °C for the porous carbon. Approximately 70 mg of the carbon was evacuated at 5 mTorr at 300 °C for 16 h. The measured pressure (P/P_0) was 0.05-0.999. The Brunauer-Emmett-Teller (BET) SSA was calculated using the BET theory based on the adsorption branches of the isotherms. PSDs and pore volumes were determined using the non-local density functional theory (NLDFT) method provided by data reduction software for N_2 isotherms collected at −196 °C [15]. The NLDFT model assumes slit-shaped pores with uniformly dense carbon walls; the adsorbate is considered to be a fluid of hard spheres [15]. Samples for transmission electron microscopy (TEM) were prepared by dispersing each sample in ethanol and placing the solution over a copper grid with a carbon film. A TEM study was performed using the Tecnai F20 microscope at 200 kV. X-ray diffraction (XRD) analysis was done using a Rigaku diffractometer with CuKα radiation (λ=0.154 nm) operating at 30 mA and 40 kV. XRD patterns were collected using step scans with a step size of 0.01° (2θ) and a count time of 2s per step between 5 (2θ) and 80 (2θ). Samples were analyzed by Raman spectroscopy (Renishaw 1000) using an Ar ion laser (514 nm) at 20 X magnification (~2 μm spot size), 30% defocus, and 0.6 mW power. X-ray photoelectron spectroscopy (XPS) analysis was performed on a MultiLab 2000 (Thermo) instrument with Al Kα radiation (15 kV, 150 W) under a pressure of $5*10^{-10}$ mbar.

3. Electrochemical Evaluation

To evaluate the electrochemical performance of the porous carbon composites prepared using the two processes, we fabricated 2032-type coin cells (MTI). The prepared sample was pressed onto

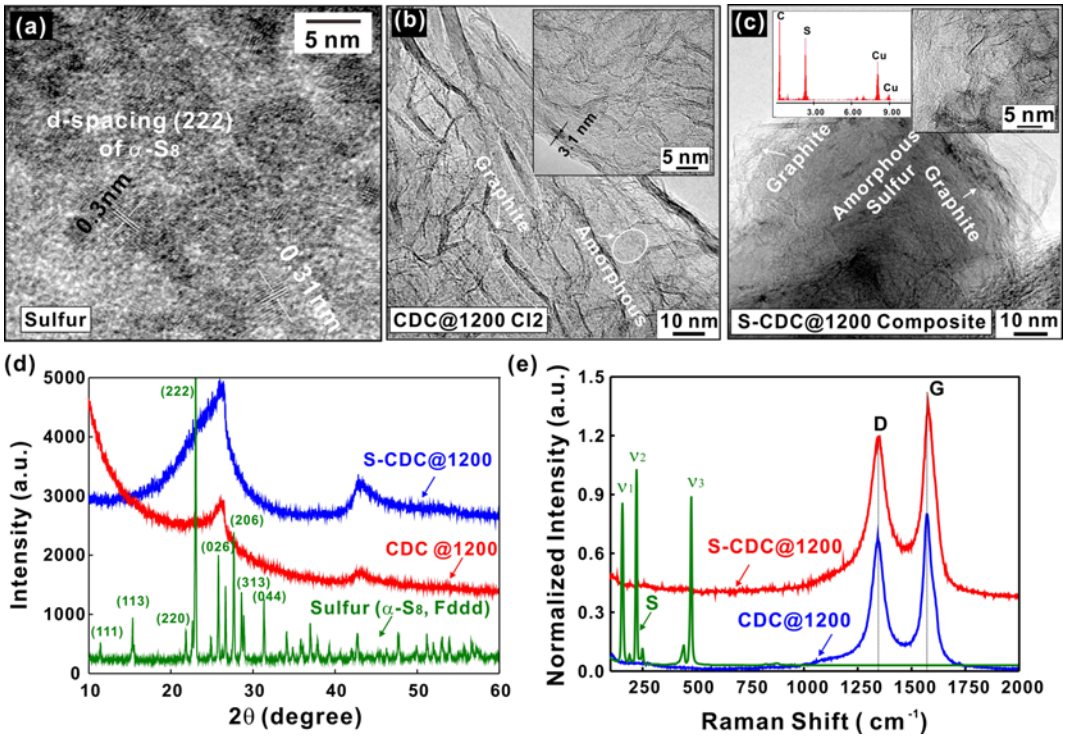

Fig. 1. TEM images (a,b,c), XRD (d), and raman (e) of pristine S powder, CDC chlorinated at 1,200 °C, and S-CDC@1200 composite.

an aluminium substrate as the working electrode, including binder and conductive additives. Li was used as the counter electrode. The separator used was Celgard[R] 3501 (microporous monolayer membrane). To inhibit the shuttling effect in the cathodes, multi-layer PP separators were implemented as physical barriers through 2, 4, and 10 stacks of one-layer PP separators. The characteristics of the separator are as follows: thickness of 25 μm, porosity of 55%, pore size of 64 nm. The specific capacities were calculated based on only the sulfur mass. The cathode electrode material was prepared by adding Super-P (10%) as a conductive additive and polyvinyl fluoride (PVDF, 10%) as a binder in all cases. The utilized electrolyte was composed of the following: 1 M of Li TFSI in 1,3-dioxolane and 1,2-dimethoxyethane (volume ratio 1 : 1), denoted as 1 M LiTFSI/DOX·DMO.

RESULTS AND DISCUSSION

Fig. 1 provides TEM images, XRD, and Raman results of the pristine sulfur powder, CDC@1200, and S-CDC@1200 composite. In Fig. 1(a), the pristine S powder exhibits crystalline structures with d-spacings (2 2 2) of a-S_8, corresponding to approximately 0.3 nm. The CDC@1200 formed highly ordered curved sheets of graphite with an interplanar spacing of approximately 0.3-0.4 nm. The amorphous carbons coexisted within the curved graphite. Micropores and mesopores were embedded in the amorphous area surrounding the graphitic region, as illustrated in Fig. 1(b). For the S-CDC@1200 composite, sulfur and CDC@1200 were mixed homogeneously without being able to distinguish the crystalline S phase from the CDC@1200 matrix. A typical XRD pattern of the CDCs chlorinated at 1,200 °C displays a strong diffraction line corresponding to the graphite (0 0 2) reflection (2θ=26.54°), which is in the pattern of the sample superimposed on a very broad peak from amorphous carbon [10]. The S-CDC@1200 composite exhibited one broad peak from amorphous S in the 2θ range of 20-25°, but there were no S crystalline peaks. The peaks corresponding to orthorhombic sulfur disappeared completely after the CS_2 extraction during the IS method. The Raman spectra (Fig. 1(e)) were normalized to the intensity of the G-band at ~1,580 cm^{-1}. In the sulfur powder, strong Raman modes were observed at 153, 217, and 471 cm^{-1}, which agrees with the previously reported values of polycrystalline S [16], and these modes were designated as ν_1, ν_2, and ν_8, respectively. This is an orthorhombic crystal built of S8 molecules, with unit cell dimensions a=1.045 nm, b=1.2884 nm, and C=2.446 nm (Powder Diffraction Card Number 8-247, International Center for Diffraction Data, Newton Square, PA, USA). The CDC@1200 exhibited a broad D band typical of amorphous disordered carbon [10,17]. S-CDC@1200 composites did not display peaks indicative of crystalline S in the range of 400-600 cm^{-1}.

Fig. 2 shows the N_2 adsorption isotherms and the estimated PSDs of CDCs obtained from the CDC-1200, determined from the N_2 sorption isotherms using the NLDFT model for slit pores. The marked hysteresis observed in the nitrogen adsorption confirms the presence of mesoporosity. High temperature of CDC@1200 led to larger pores, which can be tuned in a range from 0.5 to 4 nm (micropore +mesopore) with BET SSA, ~1,100 m^2/g.

X-ray photoelectron spectroscopy (XPS) (MultiLab 2000 Thermo)

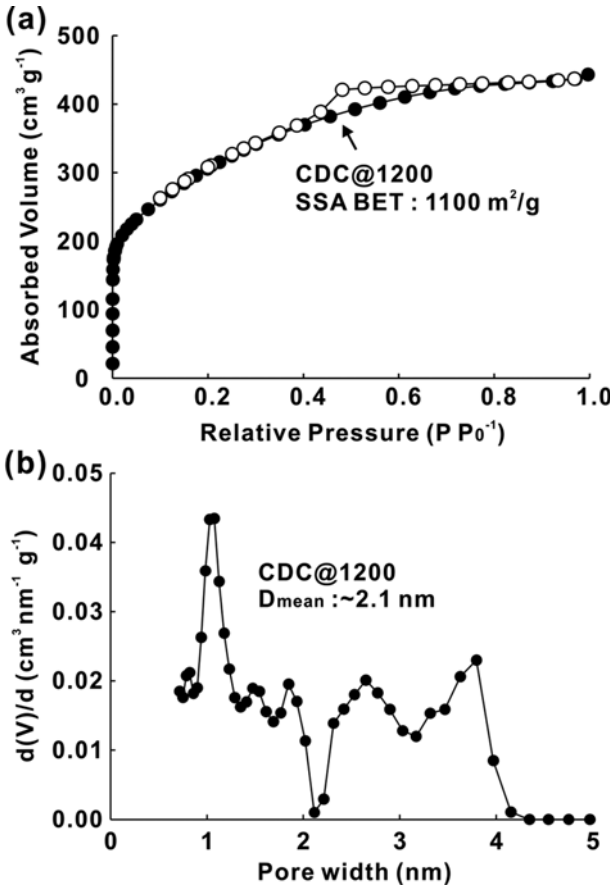

Fig. 2. (a) N_2 sorption isotherm and (b) PSDs of TiC-CDC@1200.

was employed to analyze the CDC@1200 and S-CDC@1200 composite. The C 1s XPS spectrum of the CDC@1200 (Fig. 3(a)) clearly indicates only the non-oxygenated ring C (284 eV). The carbon C 1s signal was always multicomponent; only the most intense peak was used in this work for charge compensation. The S-CDC@1200 composite has a degree of oxidation, with one component that corresponds to carbon atoms in a different functional group: the C in the C-O bonds (286 eV). The most intense sulfur line, S 2p, is asymmetric due to spin-orbit splitting. The sulfur S2p spectrum of the S element is composed of two components, one with the S2p3/2 signal at 165.3±0.2 eV (red curves) and the other with the signal at 166.1±0.2 eV (blue plot). The lower binding energy component can be attributed to the sulfur atoms in the S powder [18,19]. The higher binding energy (168-169 eV) is due to the components of sulfate or some other form of oxidized sulfur. A new peak at 164± 0.4 eV in S-CDC@1200 composites progressively appears that could be due to heterocyclic sulfur within an aromatic environment of the isotropic, non-graphitizing carbon from the porous carbon matrix [20].

The cyclic performance and voltage profiles of S-CDC@1200 electrodes (25 wt% and 40 wt% S) with separators composed of typical mono PP layer are presented in Fig. 4. In previous study, pristine S showed a poor cycling stability with a rapid discharge capacity fading. The discharge capacity showed low capacity of 240 mAh g^{-1} at 25th cycle [21,22] The discharge capacity and cycle life

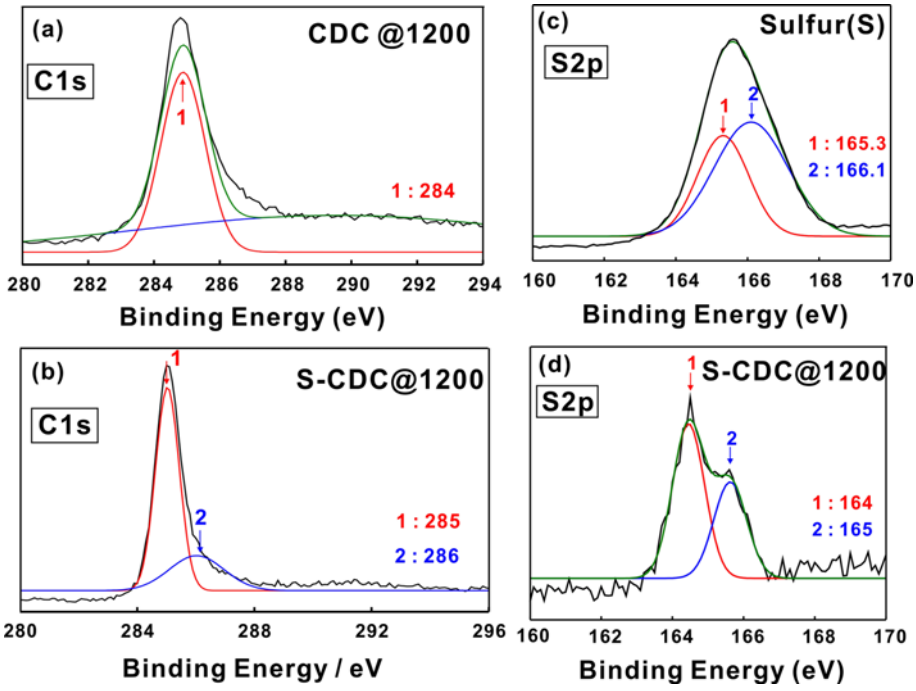

Fig. 3. The C 1s XPS spectra of (a) CDC@1200, (b) S-CDC@1200 composite, and the S2p XPS spectra of (c) Sulfur powder, (d) S-CDC@1200.

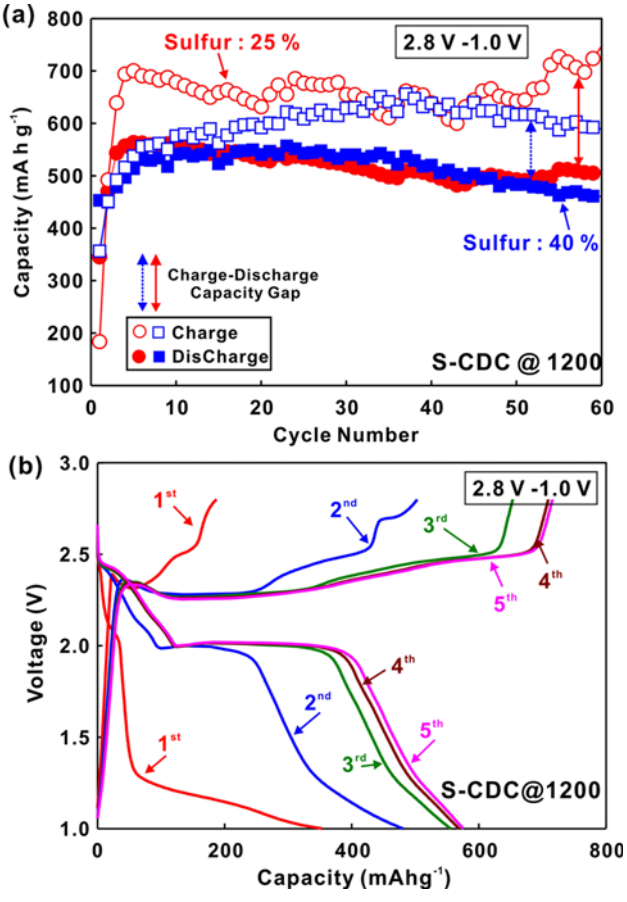

Fig. 4. The cyclic performance (a) and voltage profiles (b) of S-CDC@1200 electrodes (25 wt% and 40 wt% S) with separators composed of typical mono PP layer.

obtained with the S-CDC@1200 composite is ~500 mA h g^{-1} after 50 cycles at a rate of 0.1 C. However, a large gap in the capacity between the charge and discharge is revealed in the S-CDC@1200 composite cathode when the electrolyte *1 M LiTFSI/DOX·DMO* is used in this system. The first discharge of the S-CDC@1200 composite does not exhibit the typical two-plateau behavior (Fig. 4(b)). While the reduction of elemental sulfur (S_8) to S_6^{2-} and S_2^{2-} stages at 2.4 V and 2.03 V is very short, the conversion stage between S_2^{2-} to S^{2-} is long. Usually, the first recharge of a Li-S cell does not result in the transformation of polysulfides into elemental sulfur. During the second cycle, the plateau at 2.03 V increases gradually. As illustrated in the voltage profiles provided in Fig. 4(b), the two cathodes revealed large gaps between the charge and discharge during the second cycle. This gap is caused by the shuttling effect; the higher polysulfides diffuse to the anode where they are reduced to lower polysulfides, which diffuse back through the electrolyte to the cathode where they are reoxidized to generate higher polysulfides. Furthermore, the reaction time required for the charge operation is too long relative to the time necessary for the discharge operation. To solve this problem, the shuttle must be suppressed by a physical barrier covering the Li or inhibited by various classes of NOx compounds, like nitrate and nitrides [23]. However, the additive did not influence the reduction of the capacity gap in this study. To inhibit the shuttling effect in the cathodes of Li-S cells with high sulphur loading, multi-layered PP separators are implemented as physical barriers in place of the additives, which obstruct the migration of the produced polysulfides from the cathode to the anode. Fig. 5 depicts the cycle effects from the charge-discharge profiles of the S-CDC@1200 composite (above 50% sulfur loading) on the variations of mono- and multi-layer (2, 4, 10 layers) PP separators. In the mono-layer separator displayed in Fig. 5(a), there is a large

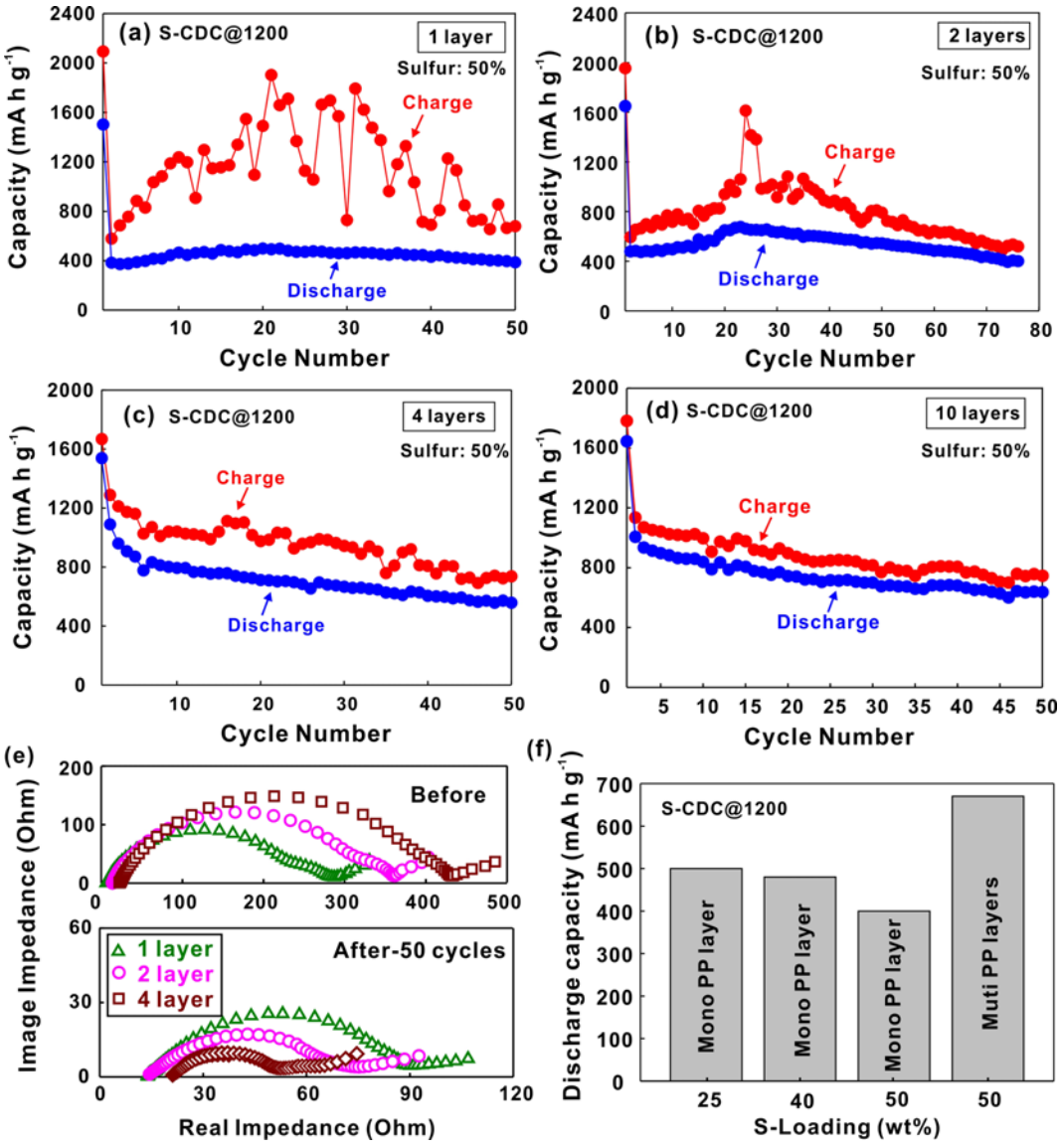

Fig. 5. Effect of cycle performance of S-CDC@1200 composite cathode with separators of: 1-10 layers (a)-(d) and impedance spectroscopy response of the cathode varying the number of separator layers before and after 50 cycles (e). Comparison of discharge capacity on the variance of S-loadings and separator layers (f).

gap between the charge and discharge capacities, indicating the presence of more serious hysteresis than in the low S-loading cathode shown in Fig. 4. Therefore, the charge-shuttle time is too long, which is indicative of a slow Li plating process for the polysulfides [24]. However, the gap gradually decreased when the number of PP separator layers, which play an important role in hindering the shuttle effect, increased, as shown in Fig, 5(b)-(d). The best discharge capacity and cycle life were obtained with ten layers of PP separator in an S-CDC@1200 composite with 50 wt% sulfur loading: 670 mA h g^{-1} after 50 cycles at a 0.1 C rate with a minimal gap in the capacities. Fig. 5(e) and Fig. 5(f) display the before and after ac impedance spectra of the Li metal/electrolyte/PP separator (1, 2, and 4)/S-CDC@1200 unit cells at room temperature. The open circuit EIS spectra of the S-CDC@1200 form a semicircle at high frequencies and an inclined tail in the low frequency region. In the initial cells (Fig. 3(e)), the interfacial resistance increased when the number of PP layers was increased before the cycling operation. The presence of additional PP layers caused an increase in the initial internal resistance of the unit cell. However, the increased resistance did not demonstrate a lower capacity at the initial stage, as indicated in Fig. 5(a)-(c). After 50 cycles, the ac impedance spectra were measured again, with results summarized in Fig. 5(e). The resistance after 50 cycles decreased more than it did for the initial cells. Additionally, the resistance of the multi-layer (2 or 4) cell was lower than the resistance of the mono-layer cell after 50 cycles. The resistance of the 10-layer cell was larger than the resistance of the 4-layer cell, but overall the resistance greatly decreased after cycling (See Fig. 1S in SI). This result indicates that the charge and discharge performance of the unit cell depends on the properties and dimensions of the separator utilized. Inhibition of the polysulfide pene-

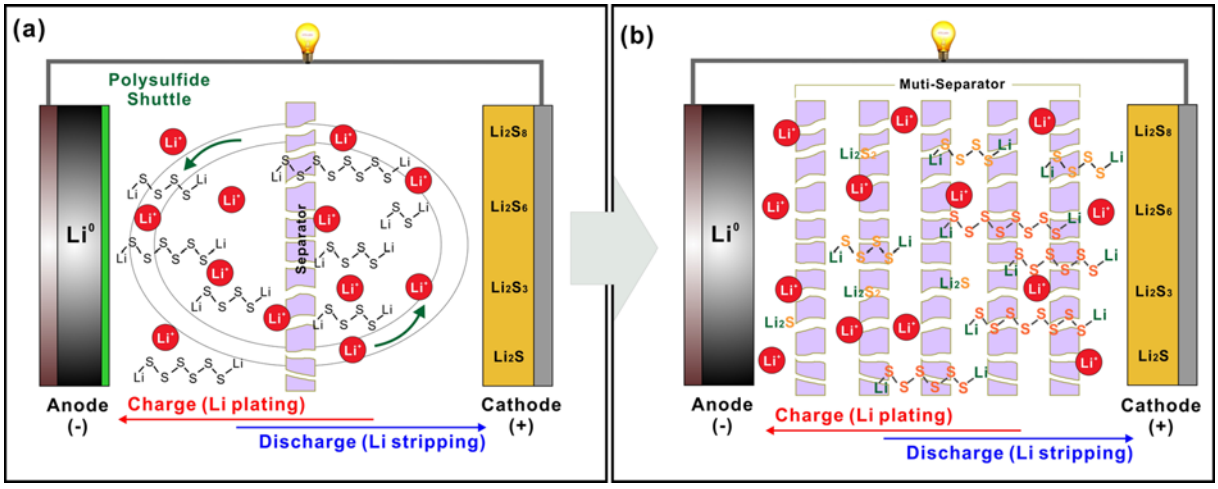

Fig. 6. Schematic diagram on shuttle effect between (a) mono- and (b) multi-layer of Li-S cell.

tration during cycling can be controlled with the separator, which is an important method for reducing the shuttling effect, as shown in the schematic diagram on shuttle effect between separators of Li-S cell (Fig. 6). Fig. 5(f) compares the discharge capacities relative to the variance of S-loadings (25 wt%, 40 wt%, and 50 wt%) and the multiple separator layers in the 50 wt%-loaded composite. As the S-loading in the composite increased from 25 wt% to 50 wt%, the discharge capacities decreased in the mono-layer separator cell from ~500 mAh g^{-1} to ~400 mAh g^{-1}, respectively, resulting in increased interfacial resistance. However, in the system using 50 wt% S-loading, the multi-layer separator significantly enhanced the discharge capacity (670 mAh g^{-1}), which is 40% higher than the discharge of the mono-layer separated cell.

CONCLUSIONS

To suppress the erosion of capacity and improve cyclic retention of lithium-sulfur batteries, tailoring the morphology of cathode materials and decreasing the shuttle effect between separator and electrolyte are essential. The cell assembly, including the cathode materials, should be specifically designed to physically block the dissolution of polysulfides and maintain electronic conductivity in the electrodes. An S-CDC@1200 composite might be appropriate for use in Li-S batteries because the porous and crystalline structures can coexist. However, high S-loading still interrupts the intrinsic electrochemical properties in the S-CDC@1200 composite. A new assembly for Li-S cells integrates multi-layer PP membranes as separators in high S-loading cathodes with a *DOX·DMO* electrolyte. The multi-layered PP separators enable the minimization of the shuttling effect by expanding the separator distance and blocking the penetration of polysulfides; therefore, the precipitation of solid Li_2S_2 and Li_2S on the two electrodes can be inhibited, indicating that the gap between the charge and the discharge capacity can be gradually decreased. The best discharge capacity and cycle life were obtained with ten layers of PP separator in an S-CDC@1200 composite (50 wt% S loading), 670 mA h g^{-1} after 50 cycles at a 0.1 C rate with minimal gap in capacity. The development of these multi-layer separator assemblies with S-CDC@1200 composites in advanced practical Li-S cells enhances the overall cell performance to exceed the current technological limits without surfactant additives in the electrolyte.

ACKNOWLEDGEMENT

This work was supported by the Next Generation Military Battery Research Center program of The Defense Acquisition Program Administration and Agency for Defense Development.

REFERENCES

1. V. S. Kolosnitsyn and E. V. Karaseva, *Russian J. Electrochem.*, **44**, 506 (2008).
2. X. Li, Y. Cao, W. Qi, L. V. Saraf, J. Xiao, Z. Nie, J. Mietek, J.-G. Zhang, B. Schwenzer and J. Liu, *J. Mater. Chem.*, **21**, 16603 (2011).
3. X. Ji, K. T. Lee and L. F. Nazar, *Nat. Mater.*, **8**, 500 (2009).
4. L. Ji, M. Rao, S. Aloni, L. Wang, E. J. Cairns and Y. Zhang, *Energy Environ. Sci.*, **4**, 5053 (2013).
5. H. Wang, Y. Yang, Y. Liang, J. T. Robinson, Y. Li, A. Jackson, Y. Cui and H. Dai, *Nano Lett.*, **11**, 2644 (2011).
6. S. Wei, H. Zhang, Y. Huang, W. Wang, Y. Xia and Z. Yu, *Energy Environ. Sci.*, **4**, 736 (2011).
7. C. Liang, N. J. Dudney and J. Y. Howe, *Chem. Mater.*, **21**, 4724 (2009).
8. C. Lai, X. P. Gao, B. Zhang, T. Y. Yan and Z. Zhou, *J. Phys. Chem. C*, **113**, 4712 (2009).
9. S.-H. Yeon, K.-N. Jung, S. Yoon, K.-H. Shin, C.-S. Jin and Y. Kim, *J. Appl. Electrochem.*, **43**, 245 (2013).
10. R. Dash, J. Chmiola, G. Yushin, Y. Gogotsi, G. Laudisio, J. Singer, J. Fischer and S. Kucheyev, *Carbon*, **44**, 2489 (2006).
11. X. Ji and L. F. Nazar, *J. Mater. Chem.*, **20**, 9821 (2010).
12. B. Scrosati and J. Garche, *J. Power Sources*, **195**, 2419 (2010).
13. J. Gao, M. A. Lowe, Y. Kiya and H. D. Abruña, *J. Phys. Chem. C*, **115**, 25132 (2011).
14. G. Zheng, Y. Yang, J. J. Cha, S. S. Hong and Y. Cui, *Nano Lett.*, **11**, 4462 (2011).
15. K. Sing, *Colloids Surf., A: Physicochem. Eng. Aspects*, **187-88**, 3

(2001).
16. R. L. Aggarwal, L. W. Farrar and D. L. Polla, *J. Raman. Spectrosc.*, **42**, 461 (2010).
17. J. Chmiola, G. Yushin, Y. Gogotsi, C. Portet, P. Simon and P. L. Taberna, *Science*, **313**, 1760 (2006).
18. M. Fantauzzi, D. Atzei, B. Elsener, P. Lattanzi and A. Rossi, *Surf. Interface Anal.*, **38**, 922 (2006).
19. H. Peisert, T. Chass, P. Streubel, A. Meisel and R. Szargan, *J. Electron. Spectrosc. Relat. Phenom.*, **68**, 321 (1994).
20. H. Marsh, P. M. A. Sherwood and D. Augustyn, *Fuel*, **55**, 97 (1976).
21. X. Liang, Z. Wen, Y. Liu, H. Zhang, L. Huang and J. Jin, *J. Power Sources*, **196**, 3655 (2011).
22. X. Liang, Y. Liu, Z. Wen, L. Huang, X. Wang and H. Zhang, *J. Power Sources*, **196**, 6951 (2011).
23. Y. V. Mikhaylik, Patent, EP1726052 B8 (2012.4.18).
24. Y. V. Mikhaylik and J. R. Akridge, *J. Electrochem. Soc.*, **151**, A1969 (2004).

Supporting Information

Carbide-derived carbon/sulfur composite cathode for multi-layer separator assembled Li-S battery

Sun-Hwa Yeon*,†, Wook Ahn*,, Kyoung-Hee Shin*, Chang-Soo Jin*, Kyu-Nam Jung*, Jae-Deok Jeon*, Sungnam Lim***, and Youngchul Kim****

*Korea Institute of Energy Research, 102, Gajeong-ro, Yuseong-gu, Daejeon 305-343, Korea
**Department of Materials Science & Engineering, Yonsei University, 50, Yonsei-ro, Seodaemun-gu, Seoul 120-749, Korea
***Department of Chemical and Biomolecular Engineering, KAIST, 373-1, Guseong-dong, Yuseong-gu, Daejeon 305-701, Korea
****Agency for Defense Development, Yuseong-gu, P. O. Box 35-4, Daejeon 305-600, Korea
(*Received 26 March 2014 • accepted 21 September 2014*)

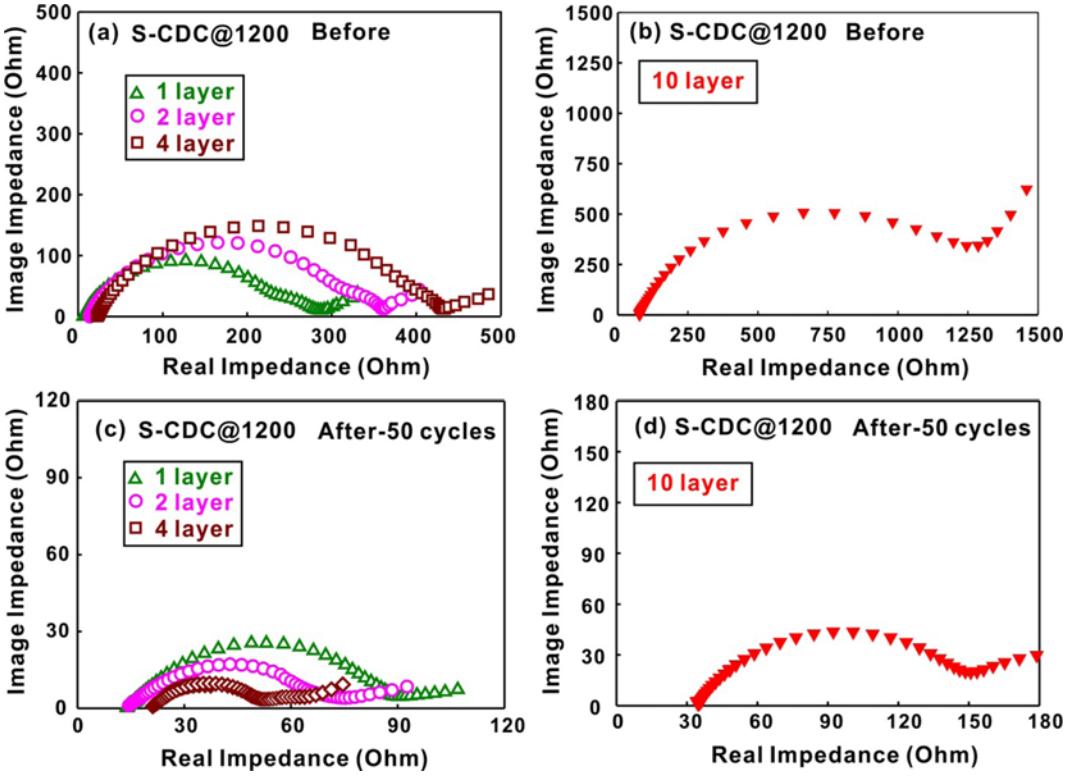

Fig. S1. Effect of cycle performance of S-CDC@1200 composite cathode with separators of: (a) 1 layer, (b) 2 layers, (c) 3 layers, and (d) 10 layers. All samples were performed at 0.1C rate.